Nuclear Engineering and Technology 54 (2022) 1175–1184

Contents lists available at ScienceDirect

Nuclear Engineering and Technology

journal homepage: www.elsevier.com/locate/net

Original Article

Fractal kinetic characteristics of uranium leaching from low permeability uranium-bearing sandstone

Sheng Zeng [a, *], Yuan Shen [a], Bing Sun [b], Kaixuan Tan [a], Shuwen Zhang [a], Wenhao Ye [a]

[a] School of Resources Environment and Safety Engineering, University of South China, Hengyang, 421001, China
[b] Civil Engineering College, University of South China, Hengyang, 421001, China

ARTICLE INFO

Article history:
Received 27 February 2021
Received in revised form
9 October 2021
Accepted 10 October 2021
Available online 14 October 2021

Keywords:
In-situ leaching
Uranium mine
Pore structure
Fractal characteristics
Leaching kinetics

ABSTRACT

The pore structure of uranium-bearing sandstone is one of the critical factors that affect the uranium leaching performance. In this article, uranium-bearing sandstone from the Yili Basin, Xinjiang, China, was taken as the research object. The fractal characteristics of the pore structure of the uranium-bearing sandstone were studied using mercury intrusion experiments and fractal theory, and the fractal dimension of the uranium-bearing sandstone was calculated. In addition, the effect of the fractal characteristics of the pore structure of the uranium-bearing sandstone on the uranium leaching kinetics was studied. Then, the kinetics was analyzed using a shrinking nuclear model, and it was determined that the rate of uranium leaching is mainly controlled by the diffusion reaction, and the dissolution rate constant (K) is linearly related to the pore specific surface fractal dimension (D_S) and the pore volume fractal dimension (D_V). Eventually, fractal kinetic models for predicting the in-situ leaching kinetics were established using the unreacted shrinking core model, and the linear relationship between the fractal dimension of the sample's pore structure and the dissolution rate during the leaching was fitted.

1. Introduction

At present, three uranium mining methods, i.e., in-situ leaching, surface heap leaching, and in-place leaching of blasted ore, are mainly adopted, among which in-situ leaching is a new and efficient uranium mining method. In-situ leaching is not applicable to all ore deposits and is only applicable to ores with porous fractures or pore development and a certain permeability. Generally, the ore body is required to be distributed in an aquifer, the ore bed must be confined and contain water. During the in-situ leaching of uranium-bearing deposits, the leaching solution is directly injected into the uranium-bearing water deposit through liquid injection boreholes to react with the minerals, and then, the solution is brought to the surface through pumping boreholes. Finally, the valuable uranium and its compound products are extracted from the pumped solutions. This mining technique is a solid-liquid transfer process that transfers useful elements from the ore into the leaching solution. This technique has been widely used for uranium leaching in China, Eastern Europe, the former Soviet Union, the United States, and Australia. In situ leaching of uranium has become the main source of uranium resources in all countries. Kazakhstan has been the most successful in using in-situ leaching and has become the largest uranium producer through ISL Kazakhstan. More than 70% of the uranium mines in the United States and Canada use in-situ leaching. The research on the in-situ leaching of uranium can be divided into three main categories: theoretical research [1], laboratory experiments [2], and numerical simulations (e.g., reactive transport modelling) [3]. At present, China's uranium resources are limited, and the uranium mining cannot meet the current energy supply demand. Through additional mining and recovery of uranium resources, mastering the original uranium leaching method is the key to China's energy security [4]. According to a July 2014 report by the World Nuclear Association (WNA), in-situ leaching is used to extract 47% of the uranium mined worldwide [5,6]. Compared with traditional uranium mining methods, in-situ leaching has many advantages such as low costs, fewer miners coming in contact with radiation, less pollution to the environment around the mining area, no solid tailings, a simple operation process, easy management, and a high utilization rate of low-grade uranium. However, it is limited by the geological and

* Corresponding author.
E-mail address: usczengs@126.com (S. Zeng).

https://doi.org/10.1016/j.net.2021.10.013

hydrogeological conditions of the sediments, especially the pore structure and permeability of the uranium-bearing layers [7–9].

Therefore, it is essential to study the influence of the pore structure characteristics of sandstone uranium deposits on the uranium leaching performance. Currently, there are many experimental methods for studying the pore structures of ore samples, such as mercury injection capillary pressure tests (MICP) [10,11], nitrogen adsorption (N2GA) tests [12,13], nuclear magnetic resonance (NMR) analysis [14,15], scanning electron microscopy (SEM) [16,17], and computed tomography (CT) analysis [18,19]. In China, since Xie [20] demonstrated that a portion of the rock pores have fractal characteristics, many scholars have conducted quantitative and qualitative characterization of the pore structures of rocks by combining experimental methods and fractal theory. For example, Guo et al. [21] found that the pore structure of tight sandstone is complex and heterogeneous, and the pore size is different, exhibiting multi-fractal characteristics. Wang et al. [22] used the mercury intrusion method (MIP) to determine the pore size distribution (PSD) of tight sandstone, studied the correlation between the PSD fractal dimension and the physical properties of tight sandstone, and developed an optimal fractal model for stratigraphic evaluation. In addition, the study of uranium leaching kinetics is an important research topic that reveals the mechanisms controlling the leaching process, and many scholars have obtained rich results on this topic. Zeng et al. [23] studied the effect of the fractal distribution on uranium leaching and showed that the shape and size of the different rock particles have unique fractal characteristics and the leaching rate is correlated to the fractal dimension. Through acid leaching of high-phosphorus hematite, Wang et al. [24] found that the kinetics of both stages of the acid leaching process are consistent with the shrinkage core model and not shrinkage core model. Madakkaruppan et al. [25] conducted microwave-assisted uranium leaching from low-grade Indian ores and showed that the kinetics of the leaching are consistent with the shrinkage core model, with product layer diffusion as the controlling mechanism. Tanaydn et al. [26] optimized the leaching process of Smithite ore using nitric acid and established a related kinetic model. Dexin et al. [27] studied the influence of the fractal dimension of the particle size distribution on the uranium leaching performance of the column leaching method and established a kinetic model of the heap leaching fractal of uranium ore with the fractal dimension changing with the particle size distribution.

These studies have investigated the pore structure of sandstone, the leaching kinetics of sandstone uranium deposits, and the influence of the fractal dimension of the particle size distribution on the leaching performance. Thus far, no one has investigated the relationship between the fractal characteristics of the pore structure and the leaching kinetics of uranium-bearing sandstone deposits. In this study, the samples collected from a uranium-bearing deposit in Xinjiang, China. The pore structure of uranium-bearing sandstone was characterized through mercury intrusion experiments. These ores were conducted a column leaching experiment to study the influence of the fractal characteristics of the pore structure on the uranium leaching kinetics. Finally, establish a fractal model for predicting the kinetic processes, considering the fractal dimension of the pore structure, in the in-situ leaching of uranium.

2. Materials and method

2.1. Sample preparation

The experimental samples were collected from a uranium bearing sandstone deposit in the Kazak Autonomous Prefecture of Yili, Xinjiang, China. The uranium deposit is located in the interlayer oxidation zone in the southern margin of the Yili Basin, Xinjiang, China. Seven dry ore rock samples from seven different borehole locations in three different ore-bearing layers were selected, each with a weight of 100 g, and the samples were numbered R1–R7. In this experiment, the uranium concentrations of the uranium ore samples were determined and their uranium grades were calculated. The detailed parameters are presented in Table 1. As can be seen from Table 1, the uranium grades were 0.202–0.022 wt%, with an average of 0.05817 wt%. The grade of industrial uranium ore was reached [28].

2.2. Mercury intrusion experiments

Mercury intrusion experiments were conducted to obtain information about the pore structure parameters of the seven samples. The mercury intrusion experiments were conducted using the automatic mercury intrusion instrument (AutoporeIV9510) in the Thermal Energy Engineering Laboratory at Tsinghua University. The mercury intrusion method was first proposed by Ritter and Delek in 1945. It is based on the non-wettability of mercury on solid surfaces. It can only be squeezed into the solid pores under the action of external pressure, so the external pressure can be used as a measure of the pore size. It is generally accepted that the pores in porous solid materials are cylindrical. This model has practical significance. Because the contact angle between liquid mercury with solid materials is greater than 90° and the surface tension is very large, it is not wettable for most materials, so it is difficult for it to invade holes. The applied pressure can overcome the resistance caused by the surface tension, causing the liquid mercury to fill the pores of different sizes. The pressure required to force mercury into a pore of a given size is consistent with the Laplace formula:

$$\gamma = -2\sigma\cos\theta/p. \tag{2-1}$$

Where$\gamma$is the pore size of the porous medium, cm; $\sigma$is the surface tension of mercury, N/cm; p is the capillary pressure, that is, pressure into mercury, p; $\theta$is the liquid-solid contact angle.

2.3. Sulfuric acid leaching experiments

2.3.1. Sulfuric acid leaching experiment steps

The uranium leaching kinetics were studied through immersion tests. The leaching agent is based on the actual production situation of the mine. Sulfuric acid was selected as the leaching agent. The 1.84 g/L sulfuric acid with the purity of 98% was used to prepare a 10 g/L H_2SO_4 leaching solution. First, 7 samples (100 g) were placed in seven glass bottles. Then, 400 ml of sulfuric acid with a concentration of 10 g/L were added to each glass bottle (solid/liquid ratio of 1/4), and the bottles were gently shaken and placed on the experimental table. Rubber plugs were used to seal the bottles to prevent water evaporation and ensure the accuracy of the concentration value. The samples were taken out once every 8 h, and the uranium concentration was measured. This experiment was conducted to oxidize the tetravalent uranium to hexavalent uranium, and the chemical reaction equations are as follows:

$$2UO_2 + O_2 = 2UO_3, \tag{2-2}$$

$$UO_3 + 2H^+ = UO_2^{2+} + H_2O, \tag{2-3}$$

$$UO_2^{2+} + SO_4^{2-} = UO_2SO_4, \tag{2-4}$$

Table 1
Experimental sample parameters.

Drilling number	N126	A307	NK2-1	A204	N1406	A202	A206
Sample number	R1	R2	R3	R4	R5	R6	R7
Grade of uranium ore (wt%)	0.202	0.022	0.022	0.0435	0.020	0.078	0.0215
Uranium content (mg)	202	22	22	43.5	20	78	21.5
Sample depth interval (m)	235–245	190–200	215–225	180–190	332–342	184–194	190–200

$$UO_2SO_4 + SO_4^{2-} = UO_2(SO_4)_2^{2-}, \quad (2-5)$$

$$UO_2(SO_4)_2^{2-} + SO_4^{2-} = UO_2(SO_4)_3^{4-}. \quad (2-6)$$

2.3.2. Uranium concentration determination

In this experiment, the determination of the uranium content of the uranium ore was conducted using the titanium trichloride reduction/ammonium vanadate oxidation drop determination method [29]. A standard uranium solution with a uranium concentration of 0.1 mg/mL was prepared using U_3O_8, hydrochloric acid, and hydrogen peroxide. The determination of the uranium content was conducted using titanium oxide titration. One milliliter of standard uranium solution was placed in a 150 ml conical flask, and 12 ml of phosphate and 8 ml of water were added. Then, while the solution was constantly stirred inside a ventilation hood, three drops of titanium oxide were added, turning the solution purple; 2 drops of sodium nitrite were added, turning the solution brown; and 5 ml of urea were added, causing a large number of bubbles to form. The solution was allowed to stand for 5 min after the bubbles disappeared. After adding three drops of sodium diphenylamine sulfonate, the standard solution of an appropriate concentration of ammonium vanadate was titrated until the test solution was slightly purplish red and the color did not disappear for 30 s. Using Equations (2)–(7), the titrant of the uranium in the standard solution of ammonium vanadate was calculated, and the percentage of uranium was calculated using Equations (2)–(8).

$$T = C_1 \times V_1 / V_2. \quad (2-7)$$

where T is the titer of the standard uranium solution of ammonium vanadate (mgU/ml); C_1 is the concentration of the standard uranium solution (mgU/ml); V_1 is the volume of the standard uranium solution (ml); and V_2 is the volume of the ammonium vanadate standard solution consumed during the titration (ml).

$$C_2 = T \times V_3 / V_4 \times 1000, \quad (2-8)$$

where T is the titer of the ammonium vanadate standard solution to uranium (mgU/ml); V_3 is the volume of the ammonium vanadate standard solution consumed during the titration (ml); V_4 is the sample volume (ml); and C_2 is the concentration of uranium in the leaching solution (mg/l).

2.4. Fractal theory

The fractal dimension is an inherent quantitative measurement of irregularity and disorder. The self-compatibility with the size is an essential characteristic of a tested sample. According to the principle of fractal geometry [30], if the pore radius of the uranium ore sandstone is r, the number of pores in the sandstone with apertures of greater than or equal to r is $N(\geq r)$ [31].

$$N(\geq r) \infty r^{-D}, \quad (2-9)$$

where D is the fractal dimension of the pore structure, and D is divided into D_V and D_S. Different calculation methods have different effects on the expression of D. When the pore volume calculation method is used, D is expressed as D_V, representing the pore volume fractal dimension. When the specific surface area calculation method is used, D is expressed as Ds, which is the pore specific surface fractal dimension.

If $V(\geq r)$ is set as the volume of the pores with radii of greater than or equal to r, V_0 is the total pore volume of the sample. Research has shown that $V(\geq r)$ and V_0 has are related by the following formula [32]:

$$V(\geq r) = V_0 K_0 r^a. \quad (2\text{-}10)$$

From Equations (2)–(9) and Equation (2-10), we can obtain:

$$dN(\geq r) = K_1 r^{-D_v - 1} dr, \quad (2\text{-}11)$$

$$dV(\geq r) = K_2 r^{a-1} dr. \quad (2\text{-}12)$$

If we assume that the pores of the sandstone are approximately spherical, then

$$dV(\geq r) = K_3 r^3 dN(\geq r). \quad (2\text{-}13)$$

Then, Equation (2-11) and Equation (2-12) can be written as

$$K_4 r^{a-1} dr = K_5 r^3 r^{-D_v - 1} dr. \quad (2\text{-}14)$$

Based on Equation (2-14),

$$D_v = 3 - a. \quad (2\text{-}15)$$

From Equations (2-10) and (2-15), it can be seen that the pore volume and the pore size are related as follows:

$$V(\geq r) = V_0 K_6 r^{3 - D_v}. \quad (2\text{-}16)$$

The logarithmic expression of Equation (2-16) is

$$\lg V(\geq r) = \lg(V_0 K_6) + (3 - D_v) \lg r. \quad (2\text{-}17)$$

In the above equation, $K_i = (i = 0, 1, 2, 3, 4, 5, 6)$ are constants.

Therefore, when a scatter plot of $\lg V(\geq r)/V_0$-lgr is plotted using a double logarithmic coordinate system and linear fitting is performed, the slope of the straight line is a, and the fractal dimension of the pore volume (D_V) can be obtained from Equation (2-15).

Similar to calculating the volume of the pores, the specific surface area ($S(\geq r)$) of the pores with radii of greater than or equal to r and the total specific surface area of the sample's pores (S_0) satisfy [33]:

$$S(\geq r) = S_0 L_0 r^b. \quad (2\text{-}18)$$

By taking the derivative of Equation (2-18), we obtain

$$dS(\geq r) = L_1 r^{b-1} dr. \quad (2\text{-}19)$$

IF we assume that the pores of the sandstone are approximately spherical, then

$$dS(\geq r) = L_2 r^2 dN(\geq r). \tag{2-20}$$

By substituting this into Equation (2-19), we obtain

$$L_3 r^{b-1} dr = L_4 r^2 r^{-D_s-1} dr. \tag{2-21}$$

From Equation (2-21), it can be seen that

$$D_S = 2 - b. \tag{2-22}$$

According to the relationship between the specific surface area and the pore size, the logarithm is

$$\lg S(\geq r) = \lg(S_0 L_5) + (2 - D_S)\lg r. \tag{2-23}$$

In the above equations, $L_i = (i = 0, 1, 2, 3, 4, 5)$ are constants. Therefore, when the plot of $\lg S(\geq r)/S_0$- lgr is plotted on a double logarithmic coordinate system and linear fitting is performed, the slope of the straight line is b, and the fractal dimension of the pore surface (D_S) can be obtained from Equation (2-22).

2.5. Leaching kinetic model

The primary solid-liquid multiphase reaction is reflected by the process of uranium acid leaching. The reaction process can usually be described by the Unreacted-Core Shrinking Model (UCSM) [34,35]. From the principle of the controls of the leaching process, we know that a solid-liquid multiphase reaction mainly includes a chemical reaction control and an internal-external diffusion control. The internal diffusion control is also called solid film diffusion control, and the external diffusion control is also called liquid membrane diffusion. The following is a dynamic model of uranium leaching based on the UCSM.

We simplified the reaction in the uranium mining leaching process to

$$A_{\text{fluid}}(Leachant) + \text{bB}_{\text{solid}}(Uranium - rock) \rightarrow \text{Products}(Leachate). \tag{2-24}$$

If the reaction is controlled by liquid membrane diffusion, the reaction or dissolution fraction of the uranium in the rock can be obtained at time t as follows [27]:

$$f(t) = \frac{t}{\tau_t} = 1 - (1 - X)^{2/3}, \tag{2-25}$$

where X is the reaction or dissolution fraction of uranium (At time t, the ratio of the mass of leached metal to the mass of uranium in the sample) and X > 0. τ_t is the complete dissolution reaction time, which can be calculated using the following equation [36]:

$$\tau_t = \frac{\rho R_0^2}{2bk_{diff}C_{Afluid}}, \tag{2-26}$$

where $\rho$is the density of the uranium ore, $R_0$is the radius of the unreacted particles, $b$is a constant coefficient, k_{diff} is the diffusion coefficient, and $C_{A\ fluid}$is the concentration of the leaching solution.

If the reaction is controlled by solid membrane diffusion, the reaction or dissolution fraction of the uranium in the rock can be obtained at time t as follows [37]:

$$f(t) = \frac{t}{\tau_t} = 1 - 3(1 - X)^{2/3} + 2(1 - X). \tag{2-27}$$

If the reaction is controlled by the chemical reaction, the reaction or dissolution fraction of the uranium in the rock can be obtained at time t as follows [38]:

$$f(t) = \frac{t}{\tau_t} = 1 - (1 - X)^{1/3}, \tag{2-28}$$

where τ_t is calculated using Equation (2-26), but the diffusion coefficient (k_{diff}) is replaced by the chemical reaction coefficient ($k_{reaction}$).

3. Results and discussion

3.1. Fractal analysis of the pore structure

In terms of the pore size, different pore sizes had different effects on the permeability of the uranium-bearing sandstone. From the mercury intrusion curve data, it was found that the effective interval of the influence of the pores on the permeability varies greatly. Therefore, the fractal characteristics of the pore structure of the ore-bearing rock are discussed.

The data pairs of the pore radius (r) and the corresponding pore cumulative volume $V(\geq r)$, the pore radius (r), and the pore cumulative surface area $S(\geq r)$ of each sample were obtained. Scatter plots of $\lg V(\geq r)$versus lgr, $\lg S(\geq r)$versus lgr were plotted using a rectangular coordinate system, and linear regression fitting was performed. The fitting is shown in Figs. 1 and 2.

The relationships between the pore radius, the cumulative specific surface area, and the cumulative pore volume for the seven samples are shown in Figs. 1 and 2. As can be seen from these figures, the cumulative volume fraction, the cumulative specific surface area fraction, and the pore size of the sandstone particles were plotted using double logarithmic coordinates. There are obvious inflection points in the system. Two straight lines with different slopes were obtained through linear fitting, which shows that the distribution of this sandstone's pore structure has double fractal characteristics; that is, it has two fractal dimensions. The boundary point between the large pores and the small pores in each sample is the inflection point. The line to the left side of the inflection point represents the large pores, and the line to the right side of the inflection point represents the small pores. The large pores are the pores between the sandstone particles, and the small pores are the pores inside the sandstone particles. This pore

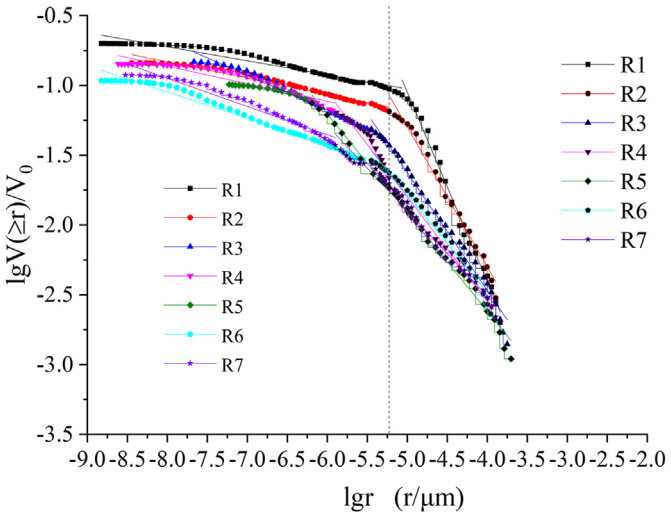

Fig. 1. Logarithmic scatter plot and linear fitting of the pore radius and the corresponding cumulative volume.

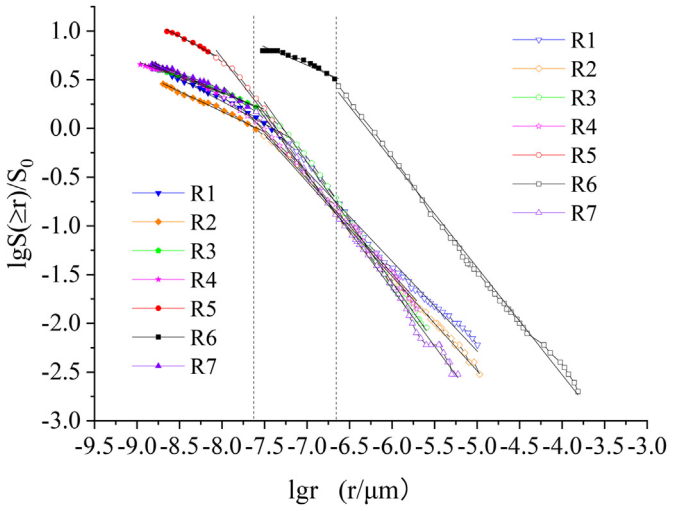

Fig. 2. Logarithmic scatter plot and linear fitting of the pore radius and the corresponding cumulative specific surface area.

distribution is related to the metallogenic process of uranium-bearing sandstone deposits. This type of uranium ore, i.e., with double fractal features, is formed by the superposition of two different metallogenic processes, geological processes, and sedimentary processes, which is consistent with the literature [39].

For the above seven samples, Equation (2-17) was used to fit the data shown in Fig. 1, and Equation (2-23) was used to fit the data shown in Fig. 2. The fractal dimension was calculated using the slope-related expression above. The corresponding pore volume fractal dimension and pore specific surface fractal dimension are shown in Table 2.

As is shown in Table 2, D_{V1}, which is the fractal dimension of the cumulative volume of the pores with large apertures, is larger than D_{V2}, which is the fractal dimension of the cumulative volume of the pores with small apertures. This demonstrates that there is a small number of large aperture pores in these sandstone samples. D_{S1} represents the fractal dimension of the specific surface area of the large pores, D_{S2} represents the integral dimension of the specific surface area of the small pores, and their ranges are 2.342–3.157. The values of D_{V1}, D_{V2}, D_{S1}, and D_{S2} have a narrow range, which indicates that the pores in these samples have similar fractal characteristics, and the value of the fractal dimension of the pore structure can reflect its degree of complexity.

3.2. Analysis of the uranium leaching rate and pore fractal dimension

Studies have shown that the macroporous structure characteristics of uranium-bearing sandstone have a greater impact on the leaching rate [40]. To vividly illustrate this effect, the influence of the pore structure characteristics of the sample on the uranium leaching was analyzed using the experimental data. As can be seen from Table 2, the structural characteristics of the seven samples are as follows: the fractal dimension of the macropore volume calculated according to the large pore diameter decreases, while the fractal dimension of the macropore specific surface area calculated according to the large pore diameter increases. As can be seen from Fig. 3, the uranium leaching rate increases with as the macropore volume fractal dimension (D_{V1}) increases. The larger the pore volume fractal dimension, the higher the leaching rate. The D_{V1} fractal dimension is proportional to the final leaching rate. As can be seen from Fig. 4, the uranium leaching rate decreases with as the larger pore surface integral shape dimension D_{S1} increases. The larger the pore surface integral shape dimension, the lower the leaching rate. The D_{S1} fractal dimension is inversely proportional to the final leaching rate.

The relationship between the leaching time and the leaching rate for the seven samples is shown in Fig. 5. It can be seen from Fig. 5 that the entire leaching process can be divided into two halves according to the intersection of the curves. The intersection is basically reached on the third day of leaching. In the first half of the leaching process, the effect of the fractal characteristics of the pore specific surface area on the leaching rate can be seen. The smaller the pore specific surface fractal dimension, the greater the leaching rate. In the second half of the leaching process, the effect of the fractal characteristics of the pore volume on the leaching rate can be seen. The larger the pore volume fractal dimension, the higher the leaching rate. The main reasons for this are as follows. In the early stage of the leaching, the leaching solution mainly reacts with the surfaces of the mineral ores, so the smaller the pore specific surface fractal dimension, the smaller the pore specific surface area, and the larger the contact area between the leaching liquid and the ore, the more fully the leaching liquid can come in contact with the ore, which speeds up the reaction and increases the leaching rate. However, in the later stage, the specific surface effect is not apparent, and it is mainly manifested by the influence of the pore volume fractal dimension. The larger the pore volume fractal dimension, the greater the porosity, and thus, more minerals are leached and the leaching rate is higher. Based on this principle, we can take corresponding measures to improve the leaching speed before and after the turning point, such as increasing the

Table 2
Fractal features of the samples' pore structure.

No.	Pore volume fractal dimension		Pore specific surface fractal dimension		Porosity
	D_{V1}	D_{V2}	D_{S1}	D_{S2}	ϕ (%)
R1	4.255	3.101	2.910	2.466	34.919
R2	3.982	3.116	2.969	2.416	39.700
R3	3.843	3.208	2.969	2.342	28.845
R4	3.748	3.125	2.992	2.358	27.369
R5	3.706	3.111	3.137	2.462	25.741
R6	3.687	3.188	3.151	2.375	24.539
R7	3.611	3.202	3.175	2.382	23.400

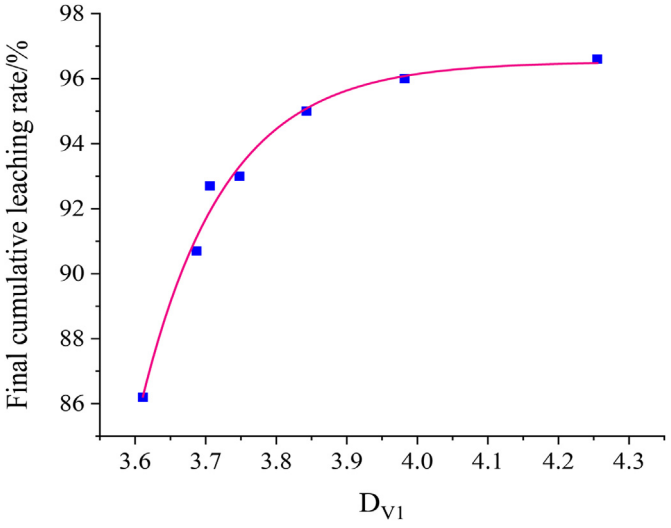

Fig. 3. Plot of the uranium leaching rate versus D_{V1}.

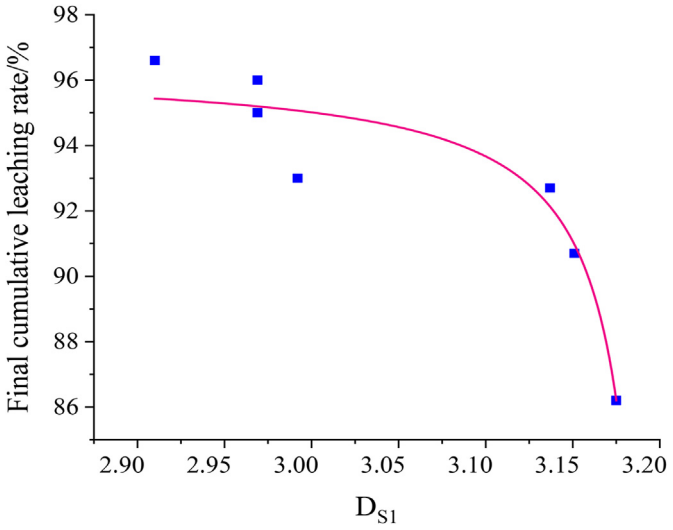

Fig. 4. Plot of the uranium leaching rate versus D_{S1}.

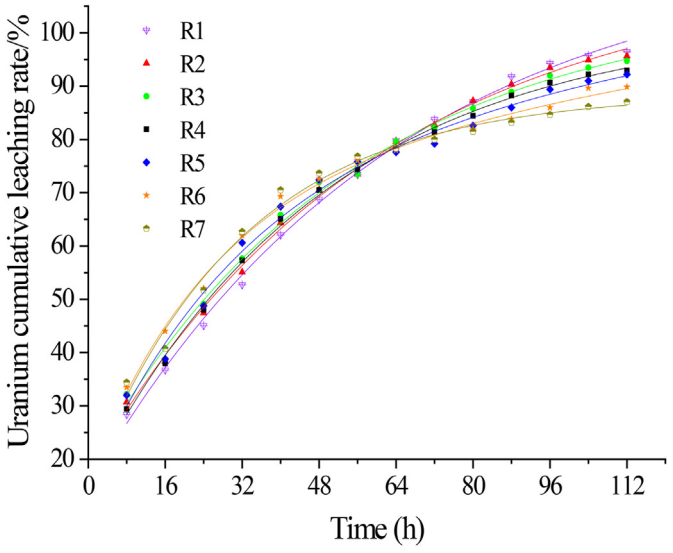

Fig. 5. Plot of Cumulative leaching rate versus leaching time.

concentration of the leaching solution in the later stage of leaching to improve the leaching rate.

3.3. Leaching kinetics

3.3.1. Comparative analysis of leaching kinetic models

During the acid leaching tests conducted on the sandstone uranium ore samples, the leached uranium concentration of the 7 ore samples at different times were measured. Next, 5 sets (R2–R6) of data were selected to analyze the kinetic characteristics of the leached uranium concentration. Equations (2-25), (2-27), and (2-28) are all linear functions of time t. A scatter plot of $(t, f(t))$ can be obtained in the y-t coordinate system. The linear fitting correlation (R-squared) and the slope of the straight line (K) can be obtained through linear fitting. The kinetic characteristics of the leached uranium concentration can be determined from the fitting correlation. By comparing how the data fits the different model, we can observe which is the most likely. Results confronted to the liquid membrane diffusion, solid film diffusion and chemical reaction are respectively shown in Figs. 6 and 7.

Espiari et al. [41] pointed out that in a leaching system, the kinetic models are difficult to distinguish. However, as can be seen from Fig. 7, the linear fitting correlation coefficient is close to 1, indicating that the solid film diffusion control of the reaction product plays a decisive role in the uranium leaching reaction system. The linear fitting correlation coefficient in Fig. 8 deviates the most from 1, indicating that the chemical reaction control does not play a decisive role in the reaction system. The correlation coefficient in Fig. 6 is between the two, indicating that the liquid membrane diffusion control plays a role in the reaction process; that is, the leaching agent diffuses to the surface of the ore and rock particles through the diffusion layer, while the uranium on the surfaces of the ore and rock particles diffuses into the leaching solution.

3.3.2. Fractal kinetic model of uranium leaching

From the above analysis of the dynamic characteristics of uranium leaching, it can be seen that the leaching rate of uranium changes significantly in the middle and later stage, which is related to the difference between the pore volume fractal dimension and the pore specific surface fractal dimension obtained from the mercury injection experiments. It can be concluded that the change in the leaching rate of uranium in the middle and later stages is probably related to the fractal dimension of the pore structure of the samples. To further explore the reasons for the differences in the later stage, the fractal dimension was introduced into the leaching kinetics of the uranium concentration, and a fractal dynamic model of uranium leaching was established. According to the research results in the literature [42–44], Equations (2-25), (2-27), and (2-28) can be written as follows:

$$1-(1-X)^{2/3} = (K_1 D + b)t, \tag{3-1}$$

$$1-3(1-X)^{2/3} + 2(1-X) = (K_2 D + b)t, \tag{3-2}$$

$$1-(1-X)^{1/3} = (K_3 D + b)t, \tag{3-3}$$

where D is the fractal dimension of the mineral rock structure; b is a constant coefficient; and K_1, K_2, and K_3 are the slopes of the liquid membrane diffusion, solid film diffusion and chemical reaction controls models respectively.

According to the kinetic fitting curves of the diffusion reaction control and chemical reaction control cases, the fitting slope of the leaching data from each group was obtained, and a slope-fractal scatter diagram was plotted. The relationship between the slope of the kinetic parameters and the fractal dimension was obtained through fitting to obtain a unified fractal dynamics equation that considers the fractal dimension. The scatter points and fitting diagrams of different control models are shown in Figs. 9–10-11. According to the slope of each fitting diagram, the three dynamic control equations, and the fractal dimension, six dynamic equations with different D_V and D_S under three control conditions are shown in Table 3.

4. Conclusions

In this study, we conducted experiments and fractal dimension analysis of the structure of uranium-bearing sandstone samples, focusing on the effects of the pore structure on acid leaching. The following conclusions were drawn.

(1) Fractal theory was combined with the results of the mercury intrusion tests conducted on the uranium-bearing sandstone

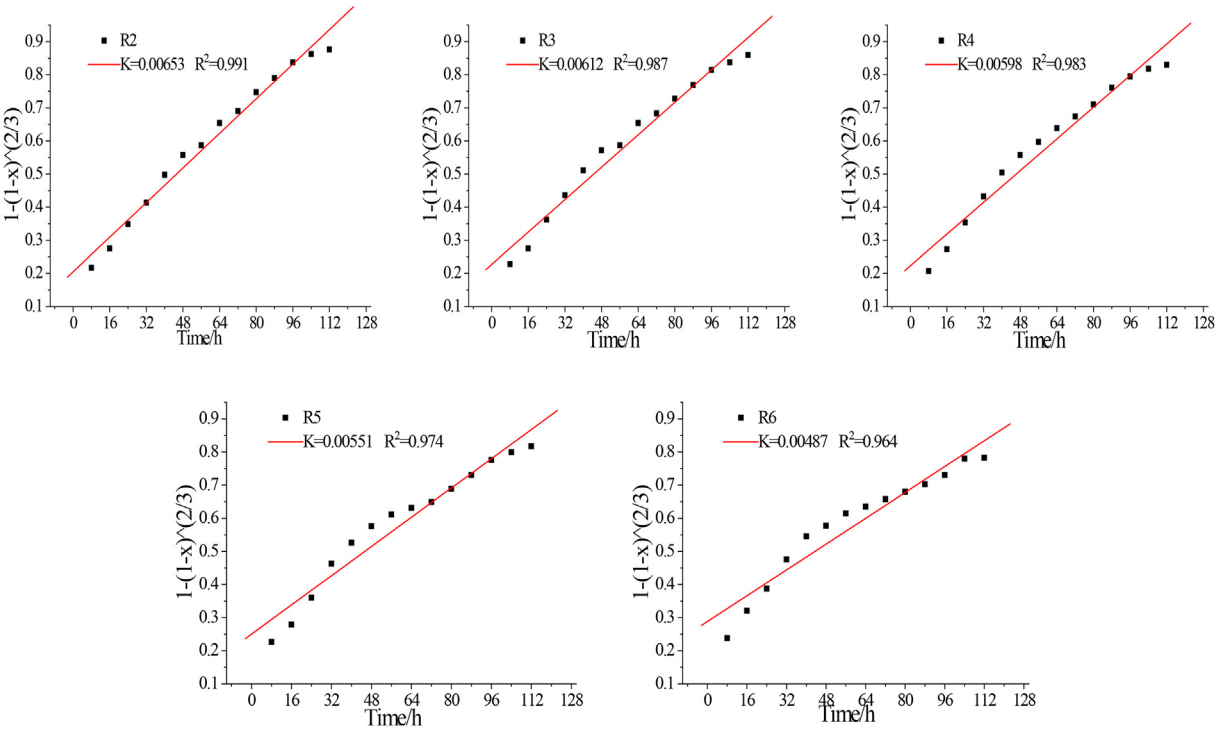

Fig. 6. Kinetic fitting diagram of the liquid membrane diffusion controlled leaching.

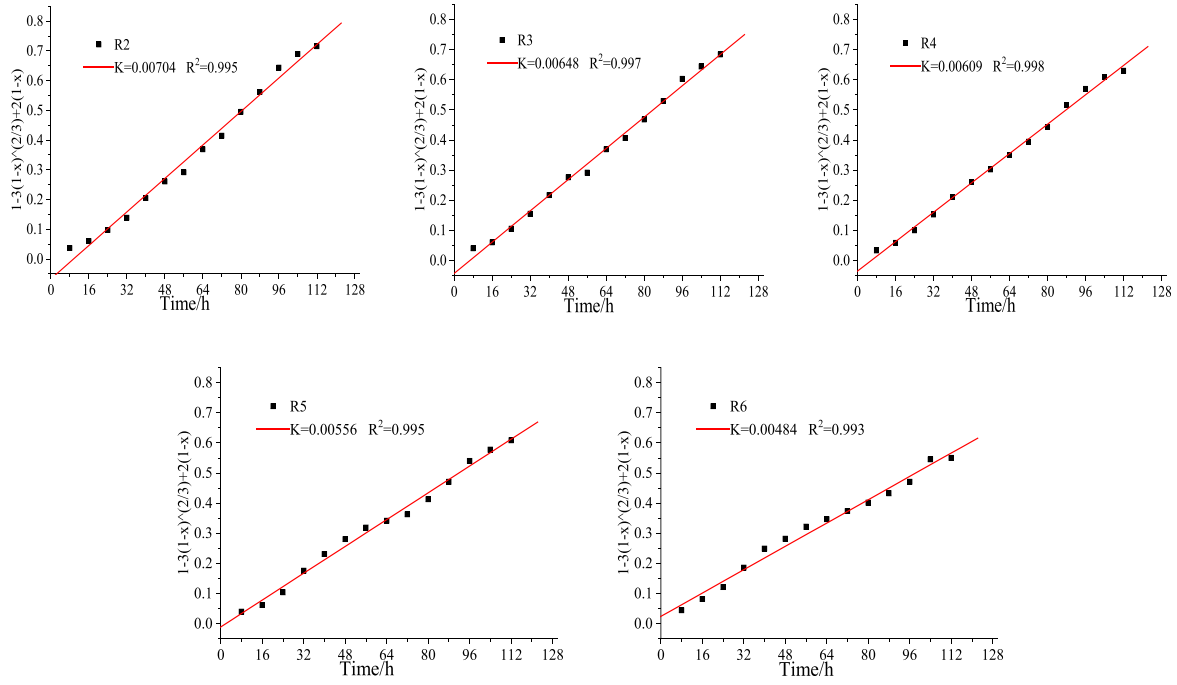

Fig. 7. Kinetic fitting diagram of the solid film diffusion controlled leaching.

ore. The logarithmic fitting plot was analyzed, and the fractal dimension value, i.e., the slope of the curve, was obtained. It was found that both the pore volume distribution and the pore specific surface area distribution have dual fractal characteristics. Among them, the porosity of the ore is mainly affected by D_{V1} rather than D_{V2}, indicating that the porosity of the sample is mainly affected by the macropores.

(2) Through the leaching tests conducted on the uranium-bearing sandstone ore samples, it was found that the pore structure characteristics of the ore have a impact on the leaching rate. Mainly based on the characteristics of the macropore structure of the ore, the effect of the pore fractal dimension of the macropores on the leaching rate was studied. It was found that the larger the fractal dimension of the volume distribution, the higher the final leaching rate;

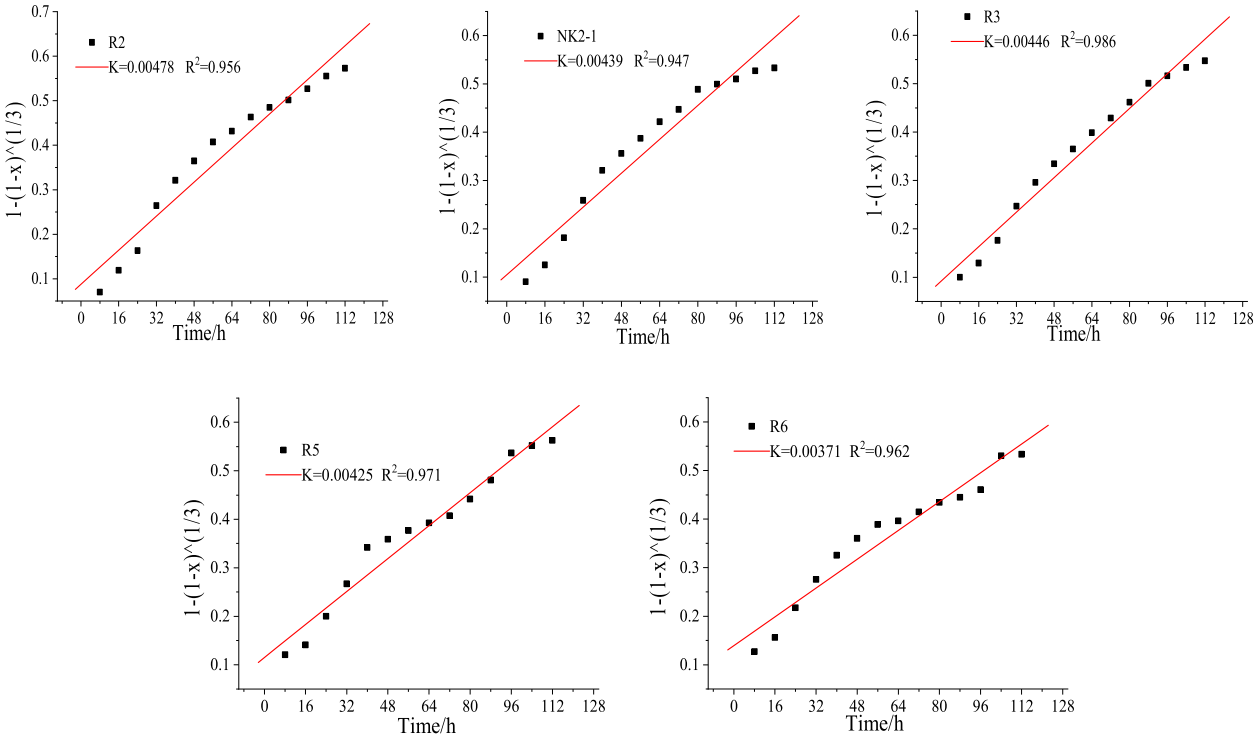

Fig. 8. Kinetic fitting diagram of the chemical reaction diffusion controlled leaching.

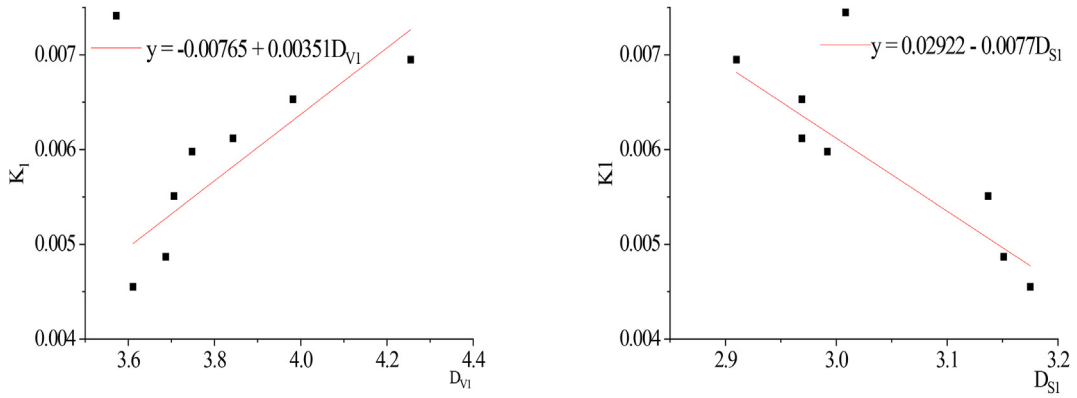

Fig. 9. The fractal dimension of the macropores versus the K_1 in the liquid film diffusion control.

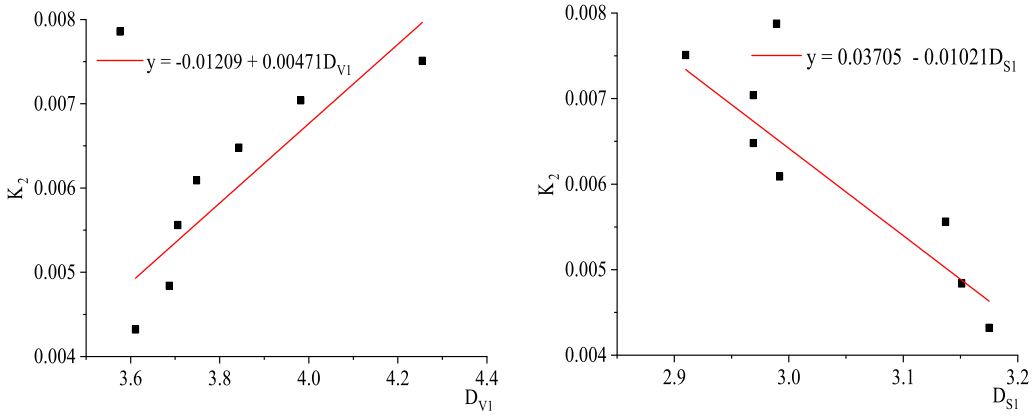

Fig. 10. The fractal dimension of the macropores versus the K_2 in the solid film diffusion control.

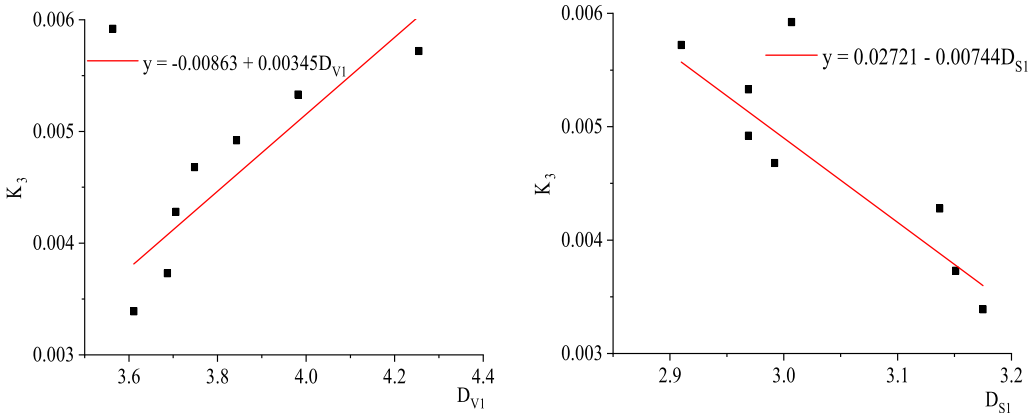

Fig. 11. The fractal dimension of the macropores versus the K_3 in the chemical reaction control.

Table 3
Uranium ore leaching fractal dynamic equation.

Reaction control type	Fractal dimension category	Leaching fractal kinetic equation
Liquid film diffusion control	Volume fractal dimension	$1-(1-X)^{2/3}=(-0.00765 + 0.00351D_{V1})t$
	Specific surface fractal dimension	$1-(1-X)^{2/3}=(0.02922-0.0077D_{S1})t$
Solid film diffusion control	Volume fractal dimension	$1-3(1-X)^{2/3}+2(1-X)=(-0.01209 + 0.00471D_{V1})t$
	Specific surface fractal dimension	$1-3(1-X)^{2/3}+2(1-X)=(0.03705-0.01021D_{S1})t$
Chemical reaction control	Volume fractal dimension	$1-(1-X)^{1/3}=(-0.00863 + 0.00345D_{V1})t$
	Specific surface fractal dimension	$1-(1-X)^{1/3}=(0.02721-0.00744D_{S1})t$

and the larger the pore specific surface fractal dimension, the lower the final leaching rate. The influence of the pore specific surface distribution characteristics on the leaching was mainly manifested in the early stage of leaching; and the influence of the pore distribution characteristics on leaching was mainly manifested in the later stage of leaching. The leaching point was basically reached on the third day of leaching.

(3) Through analysis of the uranium leaching kinetics in the uranium leaching reaction system, it was determined that the solid film diffusion control of the reaction product plays a decisive role, that is, internal diffusion. In addition, the liquid membrane diffusion also exerts an effect, that is, external diffusion. In fact, it is difficult to judge whether the leaching process is controlled in only one mechanism. It is limited by the leaching conditions such as the temperature, leaching solution concentration, ore particle size, and ore particle shape. It was concluded that only diffusion-controlled leaching applies to this type of ore acid leaching method. After determining the type of control, the fractal dimension value was introduced, and the influences of the characteristic fractal dimensions of the ore and the rock's structure on the leaching were investigated. A unified fractal dynamic characteristic equation based on the pore distribution and the pore specific surface distribution fractal dimensions was established. Analysis of the leaching fractal kinetic equation revealed that the characteristic fractal dimension of the ore's pore structure has a significant effect on the leaching effect.

Declaration of competing interest

The authors declare that they have no known competing financial interests or personal relationships that could have appeared to influence the work reported in this paper.

Acknowledgement

This study was supported by the National Natural Science Foundation of China (Grant No. 11775107).

Appendix A. Supplementary data

Supplementary data to this article can be found online at https://doi.org/10.1016/j.net.2021.10.013.

References

[1] Q. Ma, Z.G. Feng, P. Liu, X.K. Lin, Z.G. Li, M.S. Chen, Uranium speciation and in situ leaching of a sandstone-type deposit from China, J. Radioanal. Nucl. Chem. 311 (2017) 2129–2134.
[2] A.H. Orabi, S.A. Zaki, M.M. Bayoumi, D.A. Ismaiel, Leaching characteristics of uranium from el-missikat mineralized granite, J. Euro-Mediterranean Journal for Environmental Integration. 6 (1) (2021) 1–20.
[3] Lagneau Vincent, Olivier Regnault, Michaël Descostes, Industrial deployment of reactive transport simulation: an application to uranium in situ recovery, J. Reviews in Mineralogy and Geochemistry. 85 (1) (2019) 499–528.
[4] D. Shang, B. Ge Issler, M. Mew, L. Satalkina, N. Haneklaus, Unconventional uranium in China's phosphate rock: review and outlook, J. Renewable and Sustainable Energy Reviews 140 (2021) 110740.
[5] Iaea, Recent Developments in Uranium Resources and Production with Emphasis on In-Situ Leach Mining, IAEA-TECDOC, R. Vienna, Austria, 2004, p. 1396.
[6] J. Slezak, Uranium ISL mining activities at the international atomic energy agency, J. Uranium Mining and Hydrogeology (2008) 1–10.
[7] Sheng Zeng, Yuan Shen, Bing Sun, Ni Zhang, Shuwen Zhang, Feng Song, Pore structure evolution characteristics of sandstone uranium ore during acid leaching, J. Nucl. Eng. Technol. (2021), https://doi.org/10.1016/j.net.2021.06.011.
[8] L. Sinclair, J. Thompson, In situ leaching of copper:Challenges and future prospects, J. Hydrometallurgy 157 (2015) 306–324.
[9] Kaixuan Tan, Chunguang Li, L.I.U. Jiang, Huiqiong Qu, Yongmei Li, A novel method using a complex surfactant for in-situ leaching of low permeable sandstone uranium deposits, J. Hydrometallurgy 150 (2014) 99–106.
[10] J. Lai, G.W. Wang, Fractal analysis of tight gas sandstones using high-pressure mercury intrusion techniques, J. Nat. Gas Sci. Eng. 24 (2015) 185–196.
[11] P. Li, M. Zheng, H. Bi, S.T. Wu, X.R. Wang, Pore throat structure and fractal characteristics of tight oil sandstone: a case study in the Ordos Basin, China, J. Petrol. Sci. Eng. 149 (2017) 665–674.
[12] L.C. Zhang, S.F. Lu, D.S. Xiao, B. Li, Pore structure characteristics of tight sandstones in the northern Songliao Basin, China, J. Mar Petrol Geol. 88 (2017)

170–180.
[13] Z.Q. Zhang, Y.M. Shi, H. Li, W.Q. Jin, Experimental study on the pore structure characteristics of tight sandstone reservoirs in Upper Triassic Ordos Basin China, J. Energy Explor Exploit 34 (2016) 418–439.
[14] Na Zhang, Shuibing Wang, Chenggang Yan, JianJie Gao, rong Guo, hao Wang, Pore structure evolution of hydration damage of mudstone based on NMR technology, J. Journal of China Coal Society 44 (S1) (2019) 110–117.
[15] Zhentao Li, Dameng Liu, Yidong Cai, Yunpeng Wang, Guangyao Si, Evaluation of coal petrophysics incorporating fractal characteristics by mercury intrusion porosimetry and low-field NMR, J. Fuel. 263 (2020) 116802.
[16] V. Maruvanchery, E. Kim, Mechanical characterization of thermally treated calcite-cemented sandstone using nanoindentation, scanning electron microscopy and automated mineralogy, J. International Journal of Rock Mechanics and Mining Sciences 125 (2020) 104158.
[17] S.H. Yin, L.M. Wang, C.Y. Pan, X. Chen, Effect of fine interlayers on surface morphology and passivation during leaching, J. Chinese Journal of Engineering 40 (8) (2018) 910–917.
[18] Rujiang Pan, Xiang He, Weimin Xiao, Application of CT scanning technology in 3D core reconstruction, J. Research on CT Theory and Application 27 (3) (2018) 349–356.
[19] B. Bai, R. Zhu, S. Wu, et al., Multi-scale method of Nano(Micro)-CT study on microscopic pore structure of tight sandstone of Yanchang Formation, Ordos Basin, J. Pet Explor Dev. 40 (2013) 354–358.
[20] Heping Xie, Fractal geometry and its application in rock mechanics, J. Chinese Jounal of Geotechnical Engineering 14 (1) (1992) 14–24.
[21] Xiaobo Guo, Zhilong Huang, Libin Zhao, Wei Han, Ruo-mei Wang, Pore structure and multi-fractal analysis of tight sandstone using MIP, NMR and NMRC methods: a case study from the Kuqa depression, China, J. Journal of Petroleum Science and Engineering 178 (2019) 544–558.
[22] Fuyong Wang, Kun Yang, Jingxi You, Xiujie Lei, Analysis of pore size distribution and fractal dimension in tight sandstone with mercury intrusion porosimetry, J. Results in Physics 13 (2019).
[23] S. Zeng, K.X. Tan, Effect of fractal feature of the crushing size distribution on uranium leaching rate, J. Min. Metall. Eng. 31 (2011) 16–18.
[24] H.H. Wang, G.Q. Li, D. Zhao, J.H. Ma, J. Yang, Dephosphorization of high phosphorus oolitic hematite by acid leaching and the leaching kinetics, J. Hydrometallurgy 171 (2017) 61–68.
[25] V. Madakkaruppan, A. Pius, T. Sreenivas, N. Giri, C. Sarbajna, Influence of microwaves on the leaching kinetics of uraninite from a low grade ore in dilute sulfuric acid, J. Journal of Hazardous Materials 313 (2016) 9–17.
[26] M.K. Tanaydın, Z. Bakıcı Tanaydın, N. Demirkıran, Determination of optimum process conditions by central composite design method and examination of leaching kinetics of smithsonite ore using nitric acid solution, J. Sustain. Metall. 7 (2021) 178–191.
[27] Dexin Ding, Haiying Fu, Yongjun Ye, Nan Hu, Yongdong Wang, A fractal kinetic model for heap leaching of uranium ore with fractal dimension of varied particle size distribution, J. Hydrometallurgy. 136 (2013) 85–92.
[28] D.K. Nordstrom, D.W. Blowes, C.J. Ptacek, Hydrogeochemistry and microbiology of mine drainage: an update, J. Applied Geochemistry. 57 (2015) 3–16.
[29] Ministry of Nuclear Industry of the People's Republic of China, Determination of Uranium in Uranium Ore-Titanium Trichloride Reduction/Ammonium Vanadate Oxidation Titration Method, S. EJ/T 267, 1984, p. 3.
[30] X. Zhang, C. Wu, T. Li, Comparison analysis of fractal characteristics for tight sandstones using different calculation methods, J. Geophys. Eng. 14 (1) (2017) 120–131.
[31] P. Su, Z. Xia, L. Qu, W. Yu, P. Wang, D. Li, Fractal characteristics of low-permeability gas sandstones based on a new model for mercury intrusion porosimetry, J. Nat. Gas Sci. Eng. 60 (2018) 246–255.
[32] Li Peng, Min Zheng, Bi He, Songtao Wu, Xiaorui Wang, Pore throat structure and fractal characteristics of tight oil sandstone: a case study in the Ordos Basin, China, J. Petrol. Sci. Eng. 149 (2017) 665–674.
[33] A. Fw, A. Ky, B. Jy, C. Xl, Analysis of pore size distribution and fractal dimension in tight sandstone with mercury intrusion porosimetry, J. Results in Physics 13 (2019) 102283.
[34] H.S. Mohammed, Y.K. Abdel-Monem, M.G. El-Feky, S.A. Omer, M.R. Ahmed, Leaching of el-missikat low-grade fluoritized uranium ore by sulfuric acid: mechanism and kinetic, J. Radioanal. Nucl. Chem. 319 (2019) 245–255.
[35] T. A, M.E. Lasheen, H.B. El-Ahmady, A. Hassib, Oxidative leaching kinetics of molybdenum-uranium ore in h2so4 using h2o2 as an oxidizing agent, J. Frontiers of Chemical Science & Engineering 7 (2013) 95–102.
[36] Xinrui Zhu, Xuheng Liu, Zhongwei Zhao, Leaching kinetics of scheelite with sodium phytate, J. Hydrometallurgy. 186 (2019) 83–90.
[37] V. Madakkaruppan, A. Pius, T. Sreenivas, K.S. Kumar, Leaching kinetics of uranium from a quartz–chlorite–biotite rich low-grade indian ore, J. Radioanal. Nucl. Chem. 303 (2015) 1793–1801.
[38] B. Zhang, M. Li, X. Zhang, J. Huang, Kinetics of uranium extraction from uranium tailings by oxidative leaching, J. JOM. 68 (2016) 1990–2001.
[39] Z. Song, G. Liu, W. Yang, H. Zou, M. Sun, X. Wang, Multi-fractal distribution analysis for pore structure characterization of tight sandstone—a case study of the upper paleozoic tight formations in the longdong district, ordos basin, J. Marine and Petroleum Geology 92 (2018) 842–854.
[40] Bing Sun, Shituan Chen, Qinglai Zhou, Sheng Zeng, Analysis of factors affecting leaching rate during in-situ leaching of uranium, J. China, Modern Mining. 36 (8) (2020) 89–93 (in Chinese).
[41] S. Espiari, F. Rashi, S.K. Sadrnezhaad, Hydrometallurgical treatment of tailings with high zinc content, J. Hydrometallurgy. 82 (1–2) (2006) 54–62.
[42] Sheng Zeng, Jinzhu Li, Kaixuan Tan, Shuwen Zhang, Fractal kinetic characteristics of hard-rock uranium leaching with sulfuric acid, J. Royal Society Open Science. 5 (9) (2018) 19.
[43] Z. Liu, T. Xiu, Y. Du, Y. Wang, Leaching characteristics and kinetics of radioactive element uranium and thorium from ta/nb tailing, J. Radioanal. Nucl. Chem. 323 (2020) 1197–1206.
[44] J. Shen, L. Jun-Wen, Z.P. Tang, L. Yang, Leaching kinetics of uranium from waste residue by sulfuric acid with surfactant mes, J. Science Technology and Engineering 16 (11) (2016) 115–119.